The origin of hysteresis and memory of two-phase flow in disordered media

Ran Holtzman,[1] Marco Dentz,[2] Ramon Planet,[3,4] and Jordi Ortín[3,4]

[1] *Coventry University, Centre for Fluid and Complex Systems, Coventry, United Kingdom**
[2] *Institute of Environmental Assessment and Water Research (IDAEA), Spanish National Research Council (CSIC), Barcelona, Spain*
[3] *Departament de Física de la Matèria Condensada, Universitat de Barcelona, Martí i Franquès 1, Barcelona, Spain*
[4] *Universitat de Barcelona Institute of Complex Systems, Barcelona, Spain*

SUPPLEMENTARY NOTE 1: DERIVATION OF THE INTERFACE MODEL

We consider here immiscible fluid-fluid displacements in a simple disordered medium: a Hele-Shaw cell of controlled, variable gap thickness $b(x,y) = b_0 - \delta b(x,y)$, where b_0 and $\delta b(x,y)$ are the unperturbed gap thickness of the cell and its local perturbation, respectively [1]. Slowly driven flow in Hele-Shaw cells is governed by Stokes equation, since inertial forces are negligible, such that the gap-averaged velocity $\vec{u}_i(x,y)$ for each fluid ($i = 1, 2$) follows Darcy's law

$$\vec{u}_i(x,y) = -\frac{\kappa}{\mu_i}\left[\nabla p_i(x,y) - \rho_i \vec{g_e}\right], \tag{1}$$

where κ is the permeability of the cell, $\vec{g}_e = (0, g\sin\alpha)$ is effective gravity, μ_i is viscosity, ρ_i is density, and p_i is the pressure field which obeys Laplace's equation, $\nabla^2 p_i = 0$, for incompressible fluids. The interface position is given by $h(x)$, see Fig. 1 in main text. For mild deformations of the interface, $h(x) = h^0 + h^d(x)$ with $|dh^d/dx| \ll 1$, the pressure field and the velocity field can be written as $p_i = p_i^0 + p_i^d$ and $\vec{u}_i = \vec{u}_i^0 + \vec{u}_i^d$ respectively. The condition at the interface is that the pressure jump satisfies the Young-Laplace equation $[\![p]\!] = \gamma(\kappa_\parallel + \kappa_\perp)$, where γ is the interfacial tension. The out-of-plane and in-plane meniscus curvatures are approximated by $\kappa_\perp \simeq 2\cos\theta/b$ (where θ is the static contact angle) and $\kappa_\parallel \simeq d^2h/dx^2$ (to first order in h considering small interface deformations), respectively [2, 3]. Considering zero flow rate displacement where viscous effects are disregarded (referred to here as quasi-static conditions), the interface configurations are given through states of pressure equilibria. For liquid-air displacements, we obtain to a linear order in h

$$\gamma\frac{d^2h(x)}{dx^2} - \rho g\sin\alpha\; h(x) + \rho g H + p_c[x, h(x)] = 0. \tag{2}$$

The first term on the left-hand side is the contribution due to surface tension, the second term denotes the hydrostatic pressure of the wetting fluid at the interface, the third is the hydrostatic pressure at the cell inlet provided by an external reservoir (external forcing). The fourth term is the capillary pressure due to the meniscus curvature in the out-of-plane direction, $p_c(x,y) = 2\gamma\cos\theta/b(x,y)$. Here g is the gravitational acceleration, ρ the wetting fluid density, and α is the angle of inclination from horizontal.

SUPPLEMENTARY NOTE 2: HAMILTONIAN OF THE MODEL

The above equation for the sequence of interface configurations (Eq. [2]; Eq. [1] in the main text) is the result of the minimization of the following Hamiltonian functional $\mathcal{H}$ (Eq. [2] in the main text):

$$\mathcal{H}[h(x)] = \int dx \left\{ \frac{\gamma}{2}\left[\frac{dh(x)}{dx}\right]^2 + \int_0^{h(x)} dy\; [\rho g_e y - P - p_c(x,y)] \right\}, \tag{3}$$

* ran.holtzman@coventry.ac.uk

where $P = \rho g H$ is the externally imposed pressure. Solving for the Euler equation of this functional results in Eq. [2]; below we demonstrate the steps connecting both equations. Equation [3] can be rewritten as

$$\mathcal{H}[h] = \int dx\, f(h, h_x, x), \tag{4}$$

where

$$f(h, h_x, x) = \frac{\gamma}{2} h_x^2 + \rho g_e \frac{h^2}{2} - Ph - \int_0^h dy\, p_c(x, y) \tag{5}$$

and $h_x = dh/dx$. Then, $\mathcal{H}$ is minimized for $h(x)$,

$$\frac{\partial f}{\partial h} - \frac{d}{dx}\frac{\partial f}{\partial h_x} = 0, \tag{6}$$

which is the Euler equation [4]. Since $\partial f/\partial h = \rho g_e h - P - p_c(x, h)$, and $\partial f/\partial h_x = \gamma h_x$ such that the second term in Eq. [6] is equal to $\gamma d^2 h/dx^2$, Eq. [6] can be rewritten as

$$\rho g_e h - P - p_c(x, h) - \gamma \frac{d^2 h}{dx^2} = 0, \tag{7}$$

which is equal to Eq. [2].

An alternative way to link the Hamiltonian with the pressure equilibrium is as follows. First, we discretize the Hamiltonian $\mathcal{H}$ in space such that

$$\mathcal{H} = \sum_i \Delta x \left\{ \frac{\gamma}{2} \left(\frac{h_i - h_{i-1}}{\Delta x} \right)^2 + \int_0^{h_i} dy\, [\rho g_e y - P - p_c(x, y)] \right\}, \tag{8}$$

with $x_i = i\Delta x$ and $h_i = h(i\Delta x)$. In order to minimize this expression we take the derivation with respect to h_k and equate it to zero in the quasistatic limit,

$$\frac{\partial \mathcal{H}}{\partial h_k} = -\gamma \frac{h_{k+1} - 2h_k + h_{k-1}}{\Delta x^2} + \rho g_e h_k - P - p_c(x, h_k) = 0. \tag{9}$$

Taking the continuum limit of this equation makes it equivalent to Eq. [7].

SUPPLEMENTARY NOTE 3:
ANALYTICAL SOLUTION FOR THE SINGLE DEFECT

We derive here the analytical solution for the interface height $h(x)$ during imbibition and drainage for a single positive defect, which is localized in a rectangular region of width w, length ℓ and a constant elevation $\delta b > 0$; the derivation for a negative defect, $\delta b < 0$, is completely analogous. The capillary pressure is $p_c^0 = 2\gamma \cos\theta / b_0$ outside the defect and $p_c(x) = p_c^0 + a_0$ inside the defect (for $-w/2 < x < w/2$ and $d < y < d + \ell$). For compactness, we define $a_0 \equiv p_c^0 \delta b/(b_0 - \delta b)$. The full solution is obtained piecewise, that is separately for $H_e < d$ and $H_e \geq d$, where the effective height is defined as $H_e \equiv (H + p_c^0/\rho g)/\sin\alpha$. We write $h(x)$ in terms of the Green function $G(x - x')$ as [3]

$$h(x) = H_e + \int_{-\infty}^{\infty} dx' G(x - x') p_c(x', H_e), \tag{10}$$

where $G(x)$ satisfies

$$\gamma \frac{d^2 G(x)}{dx^2} - \rho g_e G(x) = \delta(x). \tag{11}$$

The solution is given by

$$G(x) = \frac{\ell_g}{2\gamma} \exp(-|x|/\ell_g), \tag{12}$$

where $\ell_g = \sqrt{\gamma/(\rho g_e)}$ is the capillary length. Inserting Eq. [12] into Eq. [10], and using the specific spatial form of $p_c(x, y)$ gives the interface solution

$$h(x) = H_e + \frac{a_0}{\rho g_e} \begin{cases} \exp(-|x|/\ell_g)\sinh(w/2\ell_g), & |x| > w/2 \\ 1 - \exp(-w/2\ell_g)\cosh(x/\ell_g), & |x| \leq w/2 \end{cases} \tag{13}$$

for $d \leq H_e < d + \ell - a_0/k$.

For $d + \ell - a_0/k < H_e < d + \ell$, we have a singular situation because the pressure perturbation at the end of the mesa defect is multi-valued, and can assume any value between 0 and a_0. This value is given by the effective defect strength, $a_e(H_e)$. It is obtained by setting $h(x = 0) = d + \ell$, which reflects the fact that the interface is pinned at $x = 0$ and $y = d + \ell$. This gives

$$a_e(H_e) = k(d + \ell - H_e). \tag{14}$$

Thus, for $d + \ell - a_0/k < H_e < d + \ell$, a_0 in Eq. [13] is replaced by a_e in Eq. [14].

During drainage, i.e. for decreasing H_e, the interface height is described by Eq. [13] as long as the defect is fully wet, i.e. for $H_e \geq H_c = d - a_0[1 - \exp(-w/\ell_g)]/\rho g_e$. In order to derive the solution for $H_e < H_c$, we consider the following differential equation for the interface height,

$$\gamma \frac{d^2h(x)}{dx^2} - \rho g_e h(x) + \rho g_e H_e + a\Theta(w/2 - |x|)\Theta[h(x) - d] = 0, \tag{15}$$

where $\Theta(x)$ is the Heaviside step function. The last Heaviside of Eq. [15] can be written as

$$\Theta[h(x) - d] = \Theta\left[w_e(H_e)/2 - |x|\right], \tag{16}$$

where the effective width $w_e(H_e)$ is defined such that $h[\pm w_e(H_e)/2] = d$. This means that the defect can be represented by an effective width $w_e(H_e)$. Note that the defect becomes weaker as it becomes narrower. Thus we do not expect that the effective width goes to zero until the release of the interface, or in other words, the interface is going to be released at finite $w_e > 0$.

The effective width can be determined as follows. First, we note that the intersects $\pm w_e/2$ between the interface $h(x)$ and the lower defect boundary for $H_e = H_c - dH_e$ can be determined from Eq. [13] as

$$h(\pm w_e/2|H_c - dH_e, w) = d. \tag{17}$$

This gives the following expression for the effective width w_e at $H_c - dH_e$, in terms of the width w,

$$w_e(H_c - dH_e) = f[H_c - dH_e, w], \tag{18}$$

where we define

$$f(H_e, w) = -2\ell_g \left\{\ln(d - H_e) + \ln(\rho g_e/a) - \ln\left[\sinh(w_e/2\ell_g)\right]\right\}. \tag{19}$$

Analogously, we obtain $w_e(H_e - dH_e)$ from $w_e(H_e)$ as

$$w_e(H_e - dH_e) = f[H_e - dH_e, w_e(H_e)]. \tag{20}$$

Thus, we obtain the following differential equation for $w_e(H_e)$

$$\frac{dw_e(H_e)}{dH_e}\left[1 - \frac{\partial f(H_e, w_e)}{\partial w_e}\right] = \frac{\partial f(H_e, w_e)}{\partial H_e} \tag{21}$$

with the initial condition $w_e(H_c) = w$. Eq. [21] can be solved by separation of variables, which gives

$$w_e(H_e) = -\ell_g \ln\left(1 - \left[1 - \exp(-w/\ell_g)\right]\frac{d - H_c}{d - H_e}\right), \tag{22}$$

Thus, for $H_0 \leq H_e < H_c$ the interface height is given by Eq. [13] where w is replaced by Eq. [22]. The interface leaves the defect at H_0, which is obtained by setting $h(x = 0) = d$.

SUPPLEMENTARY NOTE 4:
PROOF OF THE RETURN-POINT MEMORY PROPERTY

Our model satisfies the no-passing rule found by Middleton for sliding charge-density waves [5]. Front configurations, $\{h(x)\}$, can be thought as being partially ordered: If one front $\{s(x)\}$ is everywhere ahead or equal to another $\{r(x)\}$, i.e. if $s(x) \geq r(x)$ for all x, then we establish that $\vec{s} = \{s(x)\} \geq \vec{r} = \{r(x)\}$. The ordering is said to be partial in the sense that there exist front configurations that intersect each other, and for which this ordering does not apply.

The no-passing rule states that the partial ordering is preserved by the front dynamics, which is determined by the synchronous minimization of Eq. [2]. This means that if initially $\vec{s} \geq \vec{r}$, and we let $\vec{s}$ and $\vec{r}$ evolve by increasing the driving pressures P_s and P_r, respectively, with $P_s \geq P_r$ at all steps, then $\vec{s} \geq \vec{r}$ at all steps; that is, the initially more advanced configuration is never overtaken by the less advanced one.

We prove this statement by contradiction, for the case of imbibition and a positive defect, along the lines of [6] for the fluctuationless RFIM. For the other cases (negative defect, and drainage with both defect types) the proof is analogous. First, we recall the expression for the effective field,

$$p_e(x) = \gamma \frac{d^2 h(x)}{dx^2} - \rho g_e h(x) + P + p_c[x, h(x)]. \tag{23}$$

Let us assume that the above statement is false. This implies that there exists a step (value of P) at which $\vec{r}$ overtakes $\vec{s}$ for the first time at some site x, i.e. $r(x) > s(x)$. This can only occur if locally

$$p_e^r(x) > p_e^s(x), \tag{24}$$

for $r(x) = s(x)$. Note that the heights are equal just before passing, see Fig. S1a. The following observations lead to the contradiction: (i) The neighbors of $r(x)$ in the front configuration $\vec{r}$ are smaller or equal to those of $s(x)$. Thus, the in-plane curvature of $\vec{r}$ at position x is more negative than or equal to that of $\vec{s}$,

$$\gamma \frac{d^2 r(x)}{dx^2} \leq \gamma \frac{d^2 s(x)}{dx^2}; \tag{25}$$

(ii) the driving pressure is $P_r \leq P_s$ by hypothesis; and (iii) both the restoring pressure and the out-of-plane capillary pressure are equal at x, $\rho g_e r(x) = \rho g_e s(x)$ and $p_c[x, r(x)] = p_c[x, s(x)]$. Combining these observations implies that for $r(x) = s(x)$ all terms in Eq. [23] are such that the effective fields $p_e^r(x) \leq p_e^s(x)$, which is in contradiction to Eq. [24].

Since the no-passing rule has been established, the front dynamics must satisfy two additional properties for the RPM property to hold: it must be deterministic and rate-independent. The synchronous dynamics proposed for our model satisfies indeed these two properties. Our quasi-static system is rate-independent by construction. It is deterministic since any monotonic path from P_a to P_b takes the system from $\vec{a}$ to $\vec{b}$ through exactly the same sequence of front configurations.

The RPM property follows now from considering one (or more) partial cycles in which the driving pressure changes non-monotonically from P_a to P_b, see Fig. S1b. This pressure variation can be inscribed between two monotonic excursions of P from P_a to P_b, one below the nonmonotonic excursion and the other one above it. If the two monotonic excursions take the system from $\vec{a}$ to $\vec{b}$, and the no-passing rule holds, then the nonmonotonic excursion in between takes the system exactly from $\vec{a}$ to $\vec{b}$. Thus, the same final state is reached after an arbitrary number of partial cycles, proving that the RPM property of partial cyclic trajectories holds for our model.

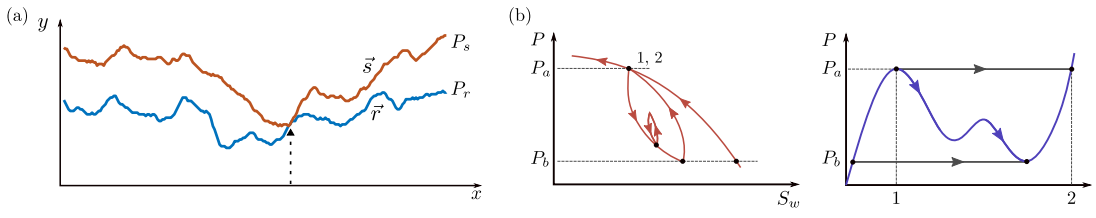

FIG. S1. Sketches of (a) the interface configurations, and (b) the 3 different excursions involved in the RPM proof.

SUPPLEMENTARY NOTE 5: EFFECT OF GRAVITY

In our system gravity plays a stabilizing role, inhibiting the size of the avalanches: following each incremental change in external pressure P, the interface moves until it reaches equilibrium, namely locally adjusts to a new Jurin's height [7]. In contrast, in typical retention experiments the sample is so small that capillary forces—which depend on the pore apertures—overwhelm those of gravity. The ratio of the gravitational pressure $P_g = \Delta\rho g l_g$ vs. that of capillarity $P_c = \gamma/l_c$ is described by the Bond number, $\mathrm{Bo} = P_g/P_c$ [8], where $\Delta\rho$ is the density difference of the two fluids. Here, the characteristic length scale for the gravitational pressure is the effective sample height $l_g = L$. The characteristic length scale for capillary pressure is the typical pore size, $l_c = a$. Thus, the Bond number is $\mathrm{Bo} = \Delta\rho g a L/\gamma$.

For our model system $a = b_0$, and the effective height is the vertical projection of the cell length, $L = L_{\mathrm{cell}} \sin\alpha$. For the simulation described in Fig. 2 in the main text, $\gamma = 20.7$ mN m^{-1}, $\Delta\rho = 998$ kg m^{-3}, $\sin\alpha = 0.0401$ (for $\alpha = 2^o21'$), $b_0 = 0.46$ mm, and $L_{\mathrm{cell}} = 80$ mm, providing $\mathrm{Bo} = 0.85$. For a typical retention experiment, considering a soil sample of length $L = 10$ mm, made of silt with pore size of $a = 0.01$ mm and similar properties γ and $\Delta\rho$, the Bond number is $\mathrm{Bo} = 0.047$, indicating the smaller importance of gravity.

To demonstrate the effect of gravity we decrease the Bond number by decreasing the tilt angle α. As α decreases the stabilizing effect of gravity decreases and avalanche sizes progressively increase, resulting in a flatter pressure-saturation (PS) curve, similar to that from typical retention experiments (Fig. S2). Sample size used here is 500×500 units; for other parameter values see *Materials and Methods* in main text.

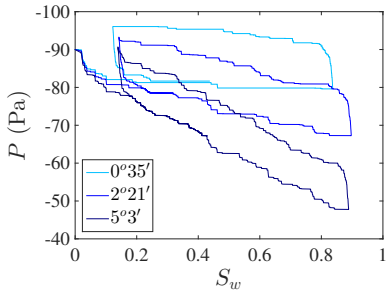

FIG. S2. Reducing Bo by decreasing the cell angle α (legend) increases the effect of capillarity, increasing the size of avalanches. This gives rise to a flatter PS curve, resembling those obtained in typical retention experiments in which capillarity is dominant over gravity (low Bo).

SUPPLEMENTARY NOTE 6: AVERAGING OVER REALIZATIONS

For practical considerations of computer runtime we limit the size of the systems in the simulations: for Fig. 4a in the main text we used sample of 400×400 units. For such small domains, the interface samples only a limited

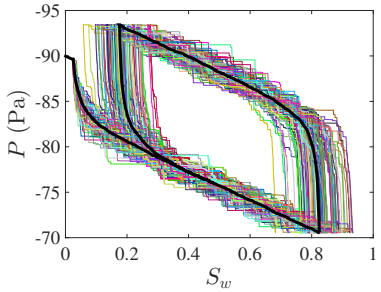

FIG. S3. Averaging over 100 realizations of samples of similar statistical properties smooths out the PS curve. The thick black line is the arithmetic mean, and the colored lines are the different realizations.

number of defect sizes, such that instabilities associated with individual defects may lead to large avalanches and a highly jugged PS curve. These effects associated with details of specific realizations of the microstructure can be alleviated by ensemble averaging, providing a smoother PS curve. Another way to smooth the data is to increase the sample size, allowing the interface to sample more values. The effect of averaging is illustrated in Fig. S3, which shows 100 realizations characterized by δp_c drawn from a Gaussian distribution with standard deviation of $\sigma_{p_c} = 11.7$ Pa centered around zero. All other parameters are identical to the typical ones used throughout the paper (see *Materials and Methods*). We find that averaging over 15 realizations (e.g. Fig. 4a) suffices to smooth out the details of particular realizations.

SUPPLEMENTARY NOTE 7:
EFFECT OF MICROSTRUCTURAL HETEROGENEITY

The data presented in Fig. 4 in the main text demonstrates the intricate effect of the microstructural heterogeneity. Specifically, Fig. 4b compares the strength of the hysteresis cycles, ΔP, for different types of microstructure: (a) Gaussian; (b) a half-sided Gaussian (positive values only); and (c) a dichotomic distribution (δp_c equal to 0 or a given positive value). We find a scaling of $\Delta P \sim (\sigma_{p_c})^n$ with $n \approx 1.4$, indicating that the macroscopic PS hysteresis depends on the distribution width rather than the specific details of the microstructure. We note that disorder could be introduced in several ways: (i) variations in defect locations; (ii) variations in defect strength δp_c; and (iii) a combination of both. In this paper we chose the latter option (iii) for most simulations, with a few additional simulations using option (i)—the dichotomic distribution in Fig. 4b.

Figure S4 provides additional data including: (1) four dichotomic distributions with various defect density (relative fraction of defects in the cell ψ); and (2) an "ordered" sample with defects placed on a regular grid, where disorder is introduced only through variations in δp_c (option ii). For completeness the three types of distributions from Fig. 4b are also shown in S4. The fact that this scaling ($n \approx 1.4$; solid line in Fig. S4) remains similar for all these types of microstructure, further extends the validity of our conclusion regarding the insensitivity of the macroscopic behavior to the details of the defect distribution. This behavior is expected to hold as long as the length of influence ℓ_g remains larger than the typical distance between the defects (which is still valid even for the most sparse sample examined here, with relative fraction of defects $\psi = 0.022$). A more detailed investigation of the impact of microstructural heterogeneity and a theoretical explanation of the value of the exponent fall beyond the scope of this paper, and remain an interesting topic for future study.

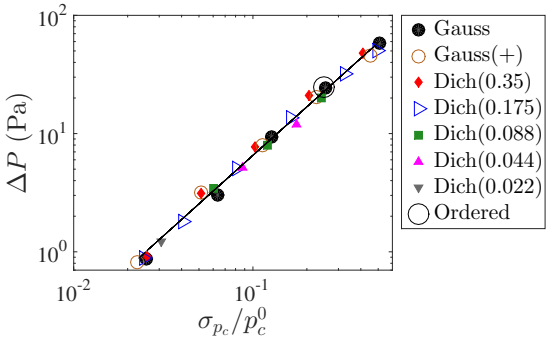

FIG. S4. The hysteresis strength ΔP (averaged pressure difference between drainage and imbibition) vs. the normalized standard deviation of the defect strength, σ_{p_c}/p_c^0, for data sets of different defect distributions, i.e. types of microstructure: (1) Gaussian (solid circles); (2) a half-sided Gaussian (positive values only; brown open circles); (3) a family of dichotomic distributions (with two values: $\delta p_c = 0$ and $\delta p_c > 0$) of various relative fraction of defects ψ (marked "Dich" in legend); and (4) ordered (defects with Gaussian distribution of δp_c placed on a square grid; large black open circle). Line indicates a linear fit of the log-log data (with slope of $n \approx 1.4$). In all cases except the ordered sample (4), the defects were placed randomly. In all cases unless indicated otherwise, the relative fraction of defects ψ was 0.35.

SUPPLEMENTARY METHODS:
PSEUDOCODE OF THE NUMERICAL IMPLEMENTATION

```
% Read simulation parameters
INPUT physical parameters: ρ, g, α, γ, δb(i,j), etc. % x = i*Δx; y = j*Δx are the spatial coordinates
INPUT run parameters: ΔH, r, h_r^*, etc.
INPUT numerical resolution and precision parameters: δh, ϵ, Δx, etc.
INITIALIZE H, S, h, p_c

% Main loop for PS trajectories; odd r (DIR=1) and even r (DIR=−1) denote imbibition and drainage
for r
    DIR = (−1)^{r+1}

    % In each run (r = 1,2,...), stop advancement once part of the interface reaches a desired height, h_r^*
    while any(DIR*(h − h_r^*) < 0)
                H = H + DIR*ΔH % increment external forcing
                COMPUTE p_e % check for equilibrium: pressure balance (Eq. 3 in main text)
                imbalance = [DIR*(p_e − ϵ) > 0] % out−of−equilibrium locations

                % iterative search for equilibrium interface configuration, h (synchronous updating)
                while any(imbalance)
                    % iteratively increment interface height (pixel−wise) until it is equilibrated
                    h(imbalance) = h(imbalance) + DIR*δh % update all out−of−equilibrium locations

                    % check if interface is touching a defect; if yes, assign the respective wetting pressure p_c
                    y_c = ceil(h/Δx)
                    for i % check each location (x) along interface
                        if δb(i,y_c(i)) ~= 0 % if touching an obstacle
                            COMPUTE δp_c(i)
                        else δp_c(i)=0
                        COMPUTE p_c(i)
                    end for

                    COMPUTE p_e % check for equilibrium: pressure balance (Eq. 3 in main text)
                    imbalance = [DIR*(p_e − ϵ) > 0] % out−of−equilibrium locations
                end while % equilibrium interface configuration h established

    end while % end of trajectory (stopping criteria h_r^* met)

    COMPUTE S(h,b) % compute saturation from interface configuration
    % store in memory saturation S, external forcing H, and interface configuration h for current equilibrium
        step
    S_all = [S_all S]
    H_all = [H_all H]
    h_all = [h_all h]
end for

% output S, H, and h at all equilibrium steps
OUTPUT S_all, H_all, h_all
```

SUPPLEMENTARY REFERENCES

[1] J. Soriano, J. Ortín, and A. Hernández-Machado, Experiments of interfacial roughening in Hele-Shaw flows with weak quenched disorder, Phys. Rev. E **66**, 031603 (2002).

[2] P. G. Saffman and G. Taylor, The penetration of a fluid into a porous medium or Hele-Shaw cell containing a more viscous liquid, Proc. R. Soc. London, Ser. A **245**, 312 (1958).

[3] R. Planet, L. Díaz-Piola, and J. Ortín, Capillary jumps of fluid-fluid fronts across an elementary constriction in a model open fracture, Phys. Rev. Fluids **5**, 044002 (2020).

[4] G. B. Arfken, H. J. Weber, and F. E. Harris, Calculus of variations, in *Mathematical Methods for Physicists* (Elsevier, 2013) pp. 1081–1124.

[5] A. A. Middleton, Asymptotic uniqueness of the sliding state for charge-density waves, Phys. Rev. Lett. **68**, 670 (1992).

[6] J. P. Sethna, K. Dahmen, S. Kartha, J. A. Krumhansl, B. W. Roberts, and J. D. Shore, Hysteresis and hierarchies: Dynamics of disorder-driven first-order phase transformations, Phys. Rev. Lett. **70**, 3347 (1993).

[7] P.-G. de Gennes, F. Brochard-Wyart, and D. Quéré, *Capillarity and Wetting Phenomena. Drops, Bubbles, Pearls, Waves* (Springer, New York, 2004).

[8] D. Wilkinson, Percolation model of immiscible displacement in the presence of buoyancy forces, Phys. Rev. A **30**, 520 (1984).